5.1. Introduction

The concept of Mott-Schottky catalysts has performed superior catalytic activity for the organic reactions. In this regard, the concept of the semiconductor nature of metal oxide and metals to form Mott-Schottky heterojunctions has been proposed and demonstrated as a viable strategy to increase catalytic activity.[1] However, the Mott-Schottky catalysts have been used in different fields such as electrocatalytic, photocatalytic, and sensor.[2] Mott-Schottky catalysts are rarely used in the field of organic transformation reactions. However, In the Mott-Schottky catalyst, charge transfer from the metal shell to metal oxide, its provides high catalytic activity and selectivity for the organic transformation reactions.[3],[4] Inspired by these results, we have explored here NiO@Ni Mott-Schottky catalyst for the amide bond formation reaction.[5],[6],[7],[8],[9],[10],[11],[12]

Recently, metal and metal oxide nanoparticles have been extensively used to study a variety of organic transformation reactions.[13],[14],[15],[16] The performance of the nanoparticles can be modulated by adjusting their size and shape, designing specific crystal phases, or increasing their surface area.[17],[18],[19] As a result, numerous techniques have been explored to achieve the desired properties of the nanoparticles.[20] Template-directed synthesis of the nanoparticles accomplishes special interest due to control in size and morphology. In addition, using a template during the nanoparticle synthesis process can improve the surface area and the number of active sites. In this respect, the use of MOF as the precursor of metallic or metal oxide nanoparticles could be important.[21],[22],[23] The MOF-derived materials improve the surface area, show high porosity, and designed morphology and crystal faces inherited from the corresponding MOF.[24],[25],[26],[27]

In this chapter, we have explored a metal-cyano coordination polymer (CP)-a subclass of

MOF as the precursor material for the synthesis of NiO@Ni Mott-Schottky catalyst.[28],[29],[30] In the CP, the metal center is interlinked through −C≡N bridges in octahedral coordination, and calcination of it in the presence of air produces NiO@Ni Mott-Schottky catalyst (see **Figure 5.1**).

In the NiO@Ni Mott-Schottky catalyst, Ni formed an amorphous layer on the surface of NiO. The conducting metallic (Ni) layer regulates the electron density within the catalyst by modulating the Fermi level charge flow. As a result, Mott-Schottky catalyst with an adjustable electron structure was formed to promote the catalytic activity.

The NiO@Ni Mott-Schottky catalyst demonstrates efficient catalysis in the coupling of different benzaldehydes and amines when used with a terminal oxidant (tert-butyl hydroperoxide, TBHP), resulting in the production of amides. The catalytic performance of the Mott-Schottky NiO@Ni catalyst is excellent that of NiO-Ni nanoparticles, which are obtained through the calcination of basic Ni^{2+}-salt. Furthermore, the NiO@Ni catalyst exhibits superior catalytic activity compared to CP-derived Ni@C and other Ni^{2+} catalysts. Furthermore,

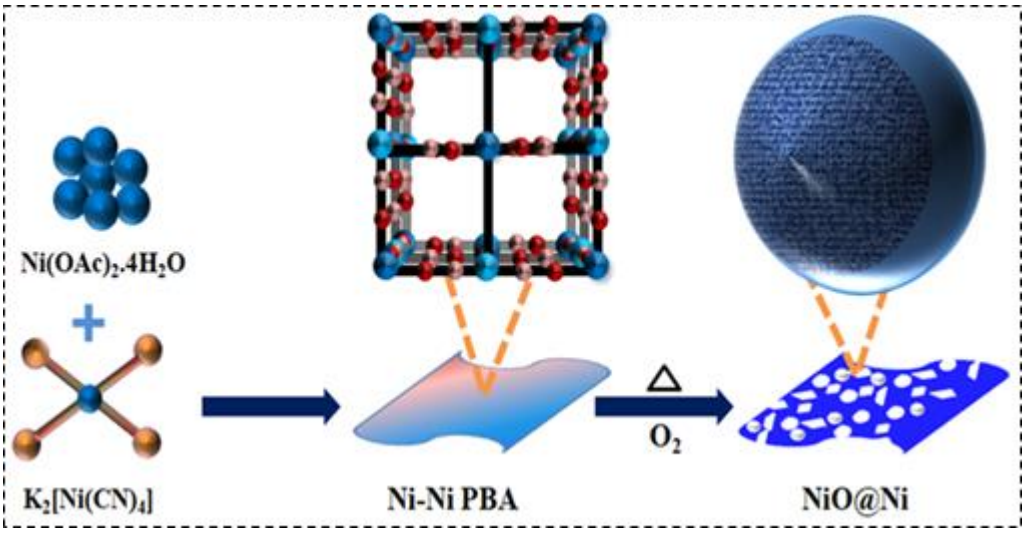

Scheme 5.1. Schematic representation for the synthesis of NiO@Ni core-shell Mott-Schottky catalyst formed by the calcination of Ni-Ni CP.

NiO@Ni can be reused up to five times with minimum lowering of its initial catalytic efficiency.

5.2. Chemicals

The aldehydes, amines, and deuterated $CDCl_3$ solvents of various substitutions were purchased from Sigma-Aldrich Pvt. Ltd. India. Nickel acetate tetrahydrate was purchased from SDFCL, Pvt. Ltd. India. The acquisition of potassium tetracyanonickelate was purchased through Sigma Aldrich, while tri-sodium citrate dihydrate was supplied by Merck Pvt. Ltd. India. These chemicals were used without any additional purification steps.

5.3. Instrumentation

The same instruments were used for the spectroscopic, microscopic, and NMR characterization of the catalysts and products as mentioned in chapter 2 section 2.3.

5.4. Experimental section

5.4.1. Synthesis of Ni−Ni CP[31]

$Ni(OAc)_2.4H_2O$ (1 mmol) and tri-sodium citrate (0.38 mmol) were dissolved in 20 mL of distilled water and stirred for 10 minute to form clear solution A. In the meantime, $K_2[Ni(CN)_4]$ (1 mmol) was dissolved separately in 20 mL distilled water and stirred 10 minute to form clear solution B. The solution B was added to solution A. Afterwards, the mixed solutions were stirred 10 minutes and sky blue precipitate appeared which was kept at room temperature for 24 h. The mixture was centrifuged at 12000 rpm to collect the precipitate followed by washing with water and acetone several times. Furthermore, the obtained precipitate was dried at 60 ^oC for overnight. As obtained the solid sample was known as Ni−Ni CP.

5.4.2. Synthesis of NiO@Ni from Ni−Ni CP[32]

Ni−Ni CP (100 mg) was ground in a mortal pastel to obtain a fine powder. The powder sample

was transferred into the crucible boat and placed inside the tumbler furnace and heating at 350 ^{o}C for 1 h (heating rate 3 ^{o}C /min from 35 ^{o}C). Afterwards, the furnace was cooled down to room temperature. Then black powder was collected and denoted as NiO@Ni nanoparticles.

5.4.3. Synthesis of NiO−Ni from $Ni(OAc)_2.4H_2O$

$Ni(OAc)_2.4H_2O$ powder was taken in a crucible boat and annealed in air at 350°C (heating rate 3°C/min) for 1 h. The furnace was allowed to cool down to room temperature. As obtained, the black color powder was denoted as NiO−Ni.

5.4.4. Synthesis of Ni@C from Ni−Ni CP[33]

The Ni−Ni CP (100) was placed in the tubular furnace and pyrolysis at 700 ^{o}C for 30 min in the nitrogen atmosphere (heating rate: 3 ^{o}C/min). The furnace was allowed to cool down to room temperature. The obtained black powder was denoted as Ni@C.

5.4.5. General procedure of amide synthesis

The amidation reaction was carried out with (1 mmol) aldehyde, (1 mmol) amine, (4 mmol) TBHP, and (5 mg) NiO@Ni in a round bottom flask with 1,4-dioxane (1 mL) as a solvent.[34],[35] The reaction was carried out under refluxing conditions in the presence of nitrogen at 60 ^{o}C for 8 h. The progress of the reaction was monitored using thin-layer chromatography to ensure completion. After completion, the reaction mixture was allowed to come down to room temperature, and the catalyst was isolated using a magnet. Next, the reaction mixture was treated with ethyl acetate and rinsed with a saturated potassium carbonate solution. The organic layer was dried using anhydrous sodium sulfate and condensed under vacuum pressure. The crude product was purified via silica gel column chromatography using a mixture of hexane and ethyl acetate.

5.5. Results and discussion

5.5.1. Characterizations of the catalyst

First, Ni−Ni CP was prepared through the reaction between nickel acetate tetrahydrate and tetracyano nickelate (II).[36] The powder X-ray diffraction (PXRD) of Ni−Ni CP was confirmed by the formation of Hofmann-type orthorhombic crystals verified with a space group of *Pnma* and cell parameters of a=12.2 Å, b=13.2 Å, and c=7.12 Å. (PXRD, **Figure 5.1a**).[36],[37] The cyanide−bridge in the PBA was also confirmed by vibrational spectroscopy. The infrared (IR) spectrum exhibited a distinct peak at 2170 cm^{-1} corresponding to the −C≡N bridges (**Figure 5.1b**).[38] Further, we have confirmed the nanoplate morphology of Ni−Ni CP by the scanning electron microscopic (SEM) study (**Figure 5.1c**).[37] Transmission electron microscopy (TEM) examination further confirmed the presence of nanoplates in Ni−Ni CP and High-resolution TEM revealed a lattice spacing of 0.34 nm, corresponding to the (311) plane of the orthorhombic crystal of PBA (with a space group: *Pnma*, **Figure 5.1d-e**).[39] The energy dispersive X-ray (EDX) spectrum demonstrated the existence of Ni, C, and N in Ni−Ni CP

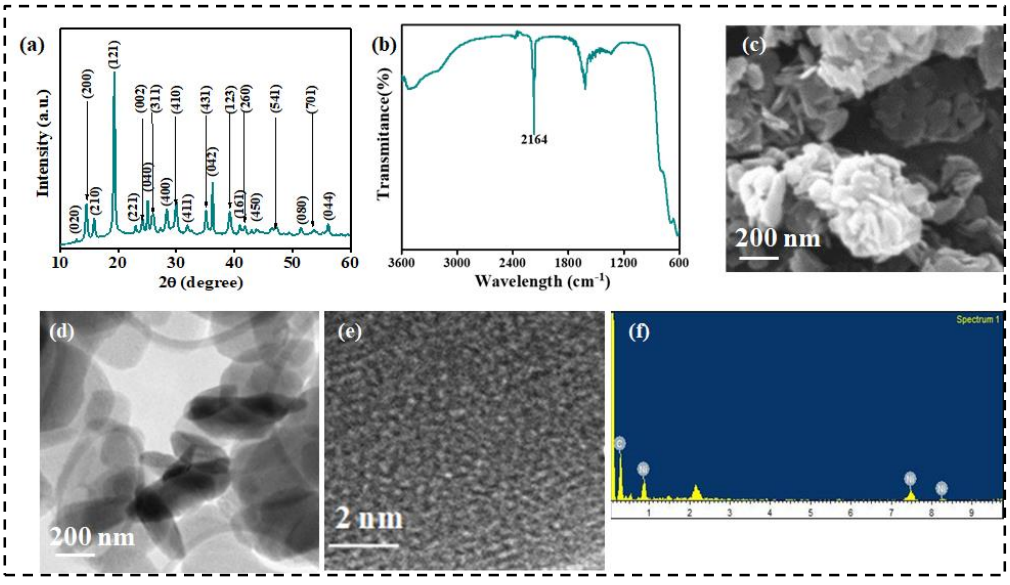

Figure 5.1. (a) and (b) images show the PXRD and FTIR spectra of the Ni−Ni CP. (d) and (e) images show the TEM and HR-TEM of the Ni-Ni PBA and (f) shows the EDX of the PBA with the Ni, C, N, and O elements.

(**Figure 5.1f**).[36]

Next, the Ni-Ni PBA was calcined at 350 °C in the presence of air to produce NiO@Ni Mott-Schottky catalyst.[40] PXRD pattern of NiO@Ni was confirmed the formation of NiO nanoparticles with cubic symmetry (space group: *Fm3m*, JCPDS no.: 04-0835, **Figure 5.2a**).[41] A broad and relatively weak peak at a 2θ value of 44.1 degree was observed, attributed to the presence of nickel.[42] The surface area of NiO@Ni nanoparticle was confirmed by the BET and determined to be 14.19 m^2/g (**Figure 5.2c**). After the calcination of PBA to NiO@Ni, morphological changes from nanoplate to spherical nanoparticles were observed by SEM images (**Figure 5.2d**). Further, TEM studies was confirmed the presence of nanoparticles consisting of a crystalline NiO core encased in a Ni shell. (**Figure 5.2e**).[36] The NiO core exhibited the size from 14 to 20 nm, while the shell thickness was determined to be between 4 and 6 nm. The Fast Fourier Transform (FFT) pattern of the shell revealed its amorphous nature, whereas the FFT of the core distinctly illustrated the crystalline structure of NiO. (**Figure 5.2g–j**). The lattice spacing of 0.24 nm within the crystalline core signified the existence of (111) planes in the cubic NiO particles.[43] The Selected Area Electron Diffraction (SAED) pattern demonstrated the polycrystalline character of the NiO core.

Further information about the core and shell was inferred from the room-temperature Raman studies of powder NiO@Ni (**Figure 5.2b**). Two peaks at 485 cm^{-1} and 1054 cm^{-1} represented

1P and 2P (P = phonon) bands of NiO nanoparticles.[44] The higher intensity of the 1P band compared to that of 2P clearly described the presence of surface defects on NiO nanoparticles.[45][46] EDX analysis of NiO@Ni showed the presence of the corresponding

elements (**Figure 5.2k-n**). The presence of ~4% carbon in NiO@Ni was also detected by elemental analysis.

Further, XPS studies determined the oxidation state and electronic configuration of the elements. (**Figure 5.2**). The Ni 2p spectrum was deconvoluted into two distinct peaks, corresponding to the Ni $2p_{3/2}$ (854.3 eV) and Ni $2p_{1/2}$ (872.2 eV). Deconvolution of the Ni $2p_{3/2}$

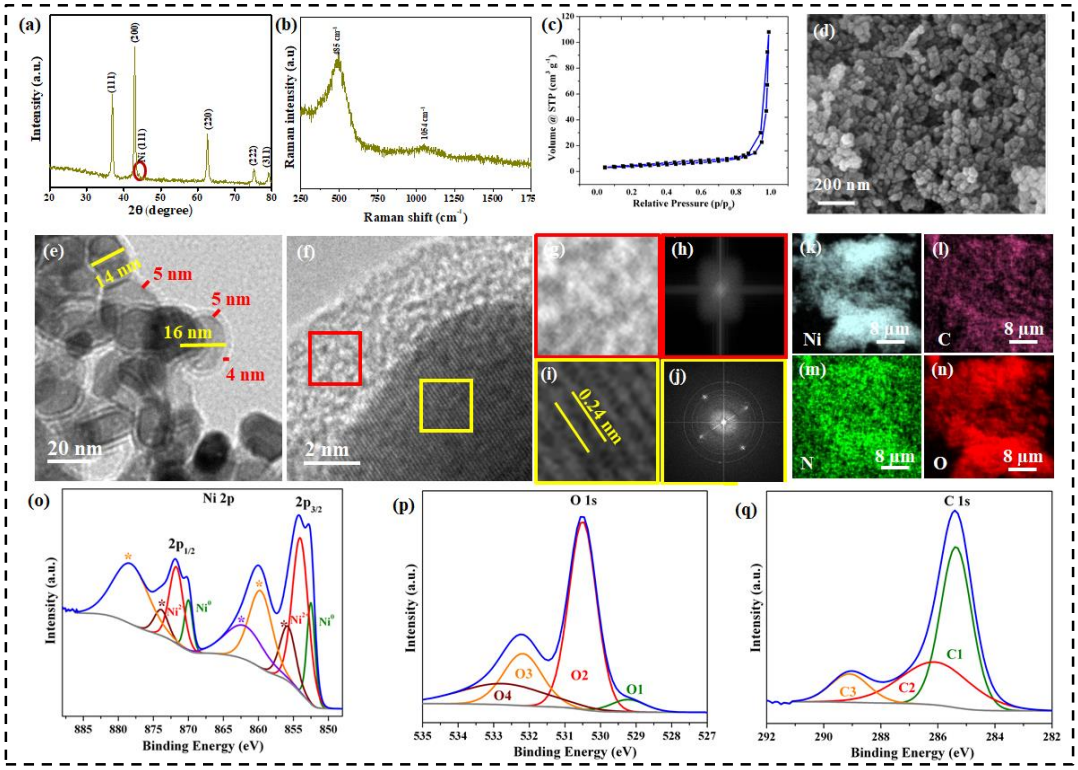

Figure 5.2. (a) & (b) image shows PXRD and Raman spectra of NiO@Ni and (c) shows the BET of NiO@Ni. (d) FE-SEM images of NiO@Ni showing spherical nanoparticles. (e) TEM image showing the thickness of the amorphous shell (4–6 nm) and NiO core (14-20 nm) and inset: selected area diffraction pattern showing polycrystalline nature of NiO, (f) HR-TEM image of NiO@Ni showing the amorphous Ni shell on the surface of the crystalline NiO nano-particles (g) magnified image of the shell, (h) corresponding FFT pattern indicating amorphous nature of the shell, (i) magnified image of the crystalline core showing the lattice spacing of 0.24 nm corresponding to (111) plane of cubic NiO and (j) corresponding FFT pattern. (k-n) Elemental mapping of NiO@Ni shows that element Ni, O, and C was homogeneously distributed. (o) This image shows the XPS spectra of Ni 2p and it was fitted into Ni^{2+} and Ni^{0} and * peaks confirmed the satellite peaks. (p) The O 1s XPS spectra deconvoluted into four peaks with corresponding Ni−O (O1), Ni−O−C (O2), and water peaks (O3 & O4). (q) The C 1s XPS spectra with corresponding C=C (C1), C−O (C2) and C=O (C3).

peak fitted into two peaks corresponding to Ni^{2+} and Ni^{0} species, while the satellite peaks at 860.2 and 862.1 eV confirmed the presence of NiO (**Figure 5.2o**).[47],[48]

The O 1s spectra was deconvoluted into four peaks corresponding to Ni−O (529.1 eV, O1), Ni−O−C (530.5 eV, O2) and adsorbed water (532.2 eV and 532.9 eV, O3 & O4) (**Figure 5.2p**).[47] C 1s spectra can be fitted into three peaks corresponding to C=C (285.1 eV), C−O (286.1 eV) and C=O (289.1 eV) species (**Figure 5.2q**).[49]

The semi-metallic NiO core and metallic Ni shell of this Mott-Schottky catalyst was found to be advantageous for enhancing the catalytic activity. The heterojunction formed between Ni and NiO fine-tuned the electron density around the catalytic sites, creating an optimal electronic environment within the catalysts to control charge transfer during catalysis. However, this interface assumes the role of a redox-active ligand in the heterogeneous catalyst, resulting in outstanding catalytic activity even without the presence of additional ligands.[50] This approach significantly reduces the overall cost of the catalytic process. Therefore, the separation of products from the catalyst can be easily separated by the simple magnetic separation method.

5.6. Optimization of reaction conditions

First, the catalytic performance of NiO@Ni was optimized for amide bond formation with a model reaction of benzaldehyde and piperidine (**Table 5.1**). Under similar reaction conditions Ni−Ni CP, Ni@C, commercial NiO, NiO−Ni nanoparticles (prepared from nickel salt) and NiO@Ni (PBA derived) produced amide in 15%, 5%, 20%, 58% and 78% yield, respectively after 12 h of reaction at 100°C (**Entries 3–7, Table 5.1**). The superior catalytic activity of the Mott-Schottky NiO@Ni catalyst can be explained by the optimized electronic environment

Table 5.1. Optimization table of the amidation reactions

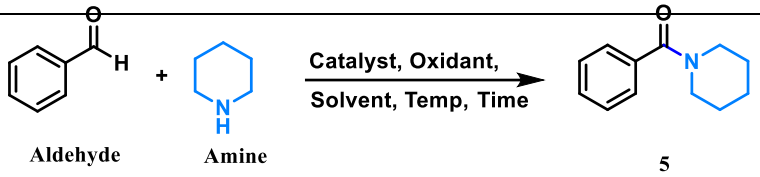

Aldehyde Amine 5

Entry	Catalyst	Oxidant	Solvent	Time (h)	Temperature (°C)	Yield (%)
Controlled reaction						
1.	-	-	Dioxane	20	100	<5
2.	-	TBHP (4 eq)	Dioxane	12	100	40
Catalysis without adding oxidant						
3.	Ni@C (5 mg)	-	Dioxane	12	100	<5
4.	NiO (commercial) (5 mg)	-	Dioxane	12	100	20
5.	NiO−Ni (5 mg)	-	Dioxane	12	100	58
6.	NiO@Ni (5 mg)	-	Dioxane	12	100	78
Catalysis with oxidant						
7.	NiO (commercial) (5 mg)	TBHP (4 eq)	Dioxane	8	60	52
8.	NiO (5 mg)	TBHP (4 eq)	Dioxane	8	60	75
9.	**NiO@Ni (5 mg)**	**TBHP (4 eq)**	**Dioxane**	**8**	**60**	**98**
10.	NiO−Ni (5 mg)	H_2O_2(4 eq)	Dioxane	8	60	85
11.	Ni@C (5 mg)	TBHP (4 eq)	Dioxane	8	60	30
Variation in catalyst amount						
12.	NiO@Ni (1 mg)	TBHP (4 eq)	Dioxane	8	60	75
13.	NiO@Ni (2 mg)	TBHP (4 eq)	Dioxane	8	60	75
14.	NiO@Ni (3 mg)	TBHP (4 eq)	Dioxane	8	60	78
15.	NiO@Ni (4 mg)	TBHP (4 eq)	Dioxane	8	60	80
16.	NiO@Ni (10 mg)	TBHP (4 eq)	Dioxane	8	60	95
17.	NiO@Ni (15 mg)	TBHP (4 eq)	Dioxane	8	60	95
Variation in TBHP amount						
18.	NiO@Ni (5 mg)	TBHP (1eq)	Dioxane	8	60	72
19.	NiO@Ni (5 mg)	TBHP (2 eq)	Dioxane	8	60	78
20.	NiO@Ni (5 mg)	TBHP (8 eq)	Dioxane	8	60	96
Variation of solvent						
21.	NiO@Ni (5 mg)	TBHP (4 eq)	DMF	8	60	50
22.	NiO@Ni (5 mg)	TBHP (4 eq)	THF	8	60	80
23.	NiO@Ni (5 mg)	TBHP (4 eq)	Water	8	60	10[$]
24.	NiO@Ni (5 mg)	TBHP (4 eq)	MeOH	8	60	30[$]

Reaction conditions: Under nitrogen atmosphere, aldehyde (1 mmol), amine (1 mmol), TBHP (4 mmol), NiO@Ni (5 mg), 1,4-dioxane (1 mL). Temperature: 60 °C, time: 8 h. [$]Acid and ester was observed as the major product instead of amide.

attained by the Fermi level manipulation at the interface. A drastic improvement of the catalytic activity (% yield, reaction temperature and reaction time) was observed after the addition of peroxide (TBHP or H_2O_2) and further optimization was carried out to obtain the optimum reaction conditions as 60°C and 8 h (**Entries 8–13, Table 5.1**). TBHP was preferred as the oxidant because higher amount of benzoic acid was detected as the byproduct when H_2O_2 was used.

The amount of catalyst also played an important role in the reaction process. 5 mg NiO@Ni was found to be an optimum amount of catalyst for 1 mmol of each reactant (**Entry 11, Table 5.1**). Reactions seem to be low yielding, incomplete at lower amount of catalyst (1–4 mg) and prolong reaction time is required (**Entries 14–17, Table 5.1**). A higher amount (10-15 mg) of catalyst did not exhibit significant improvement of the yield and reaction time (**Entries 18–19, Table 5.1**). 4 equivalents of TBHP was found to be suitable to attain the maximum yield. The higher amount of TBHP (8 equivalent) did not show significant improvement in the conversion while decreasing the amount of oxidant (1-3 equivalent) lowered the yield (**Entries 11, 20–22, Table 5.1**). A significant effect of the solvents on reaction yield and product selectivity was observed. Aprotic solvents produced better yield.

The order of yield for amidation was as follows: dioxane>THF>DMF (**Entries 11, 23–24, Table 5.1**). In protic solvents like water and methanol, major amount of benzaldehyde was converted into corresponding acid and ester, respectively, and low yield of amide was observed (**Entries 25–26, Table 5.1**). In the absence of nitrogen atmosphere, lower yield of the amide was obtained (**Entries 27, Table 5.1**).

5.7. Scope of aldehyde

After optimization of the reaction conditions, the potential of the catalyst was investigated by

synthesizing a series of amides by the reaction of amines and substituted benzaldehydes. Both the electron-rich and electron-deficient variants of benzaldehydes were found to be ideal for the formation of amides when reacting with piperidine (**Table 5.2**). In most of the cases, >92% yield was achieved under the optimized reaction conditions (**Scheme 5.1, 5a-5d, Table 5.2**). of corresponding catechol as the side product. In the case of *o*-nitro benzaldehyde, the yield of amide (88%) was slightly lower than the corresponding *para*-isomer (**Scheme 5.1, 5f-5g,**

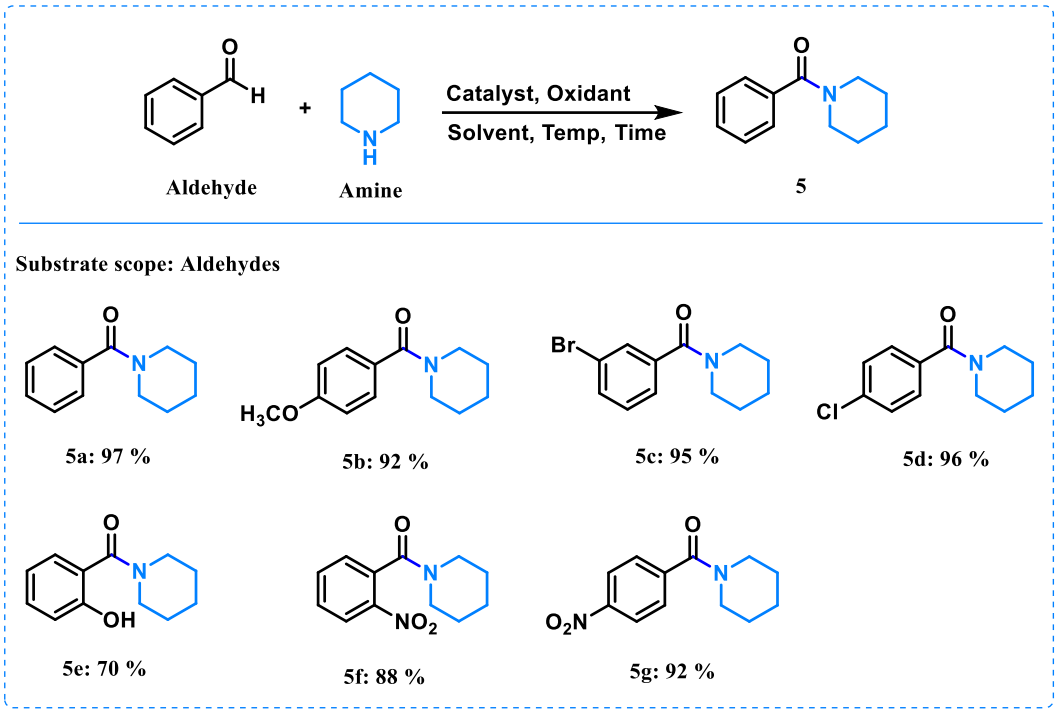

Scheme 5.2. Catalytic performance of NiO@Ni catalyst for amide bond formation. Reaction conditions: under nitrogen atmosphere, aldehyde (1 mmol), amine (1 mmol), TBHP (4 mmol), NiO@Ni (5 mg), 1,4-dioxane (1 mL). Temperature: 60 °C, time: 8 h.

Table 5.2). Although the amide formation reaction can tolerate electron-withdrawing and electron-donating functional groups such as nitro, hydroxy, methoxy, alkyl, and halogen in *ortho*-, *meta*- and *para*- positions, it is noteworthy to mention that carboxylic acid containing

benzaldehydes fail to give desired amides after multiple attempts.[51]

5.8. Scope of amine substitution

Further, the scope of different amines has been investigated under optimized reaction conditions. The conversion of secondary amines to amides was found to be more facile compared to the primary amines. A comparison of different secondary amines revealed that six-membered amines showed better conversion than the corresponding five-membered amines (**Scheme 5.2, 5aa-5ac, Table 5.2**). Further, the reaction well tolerates *meta*- and *para*-

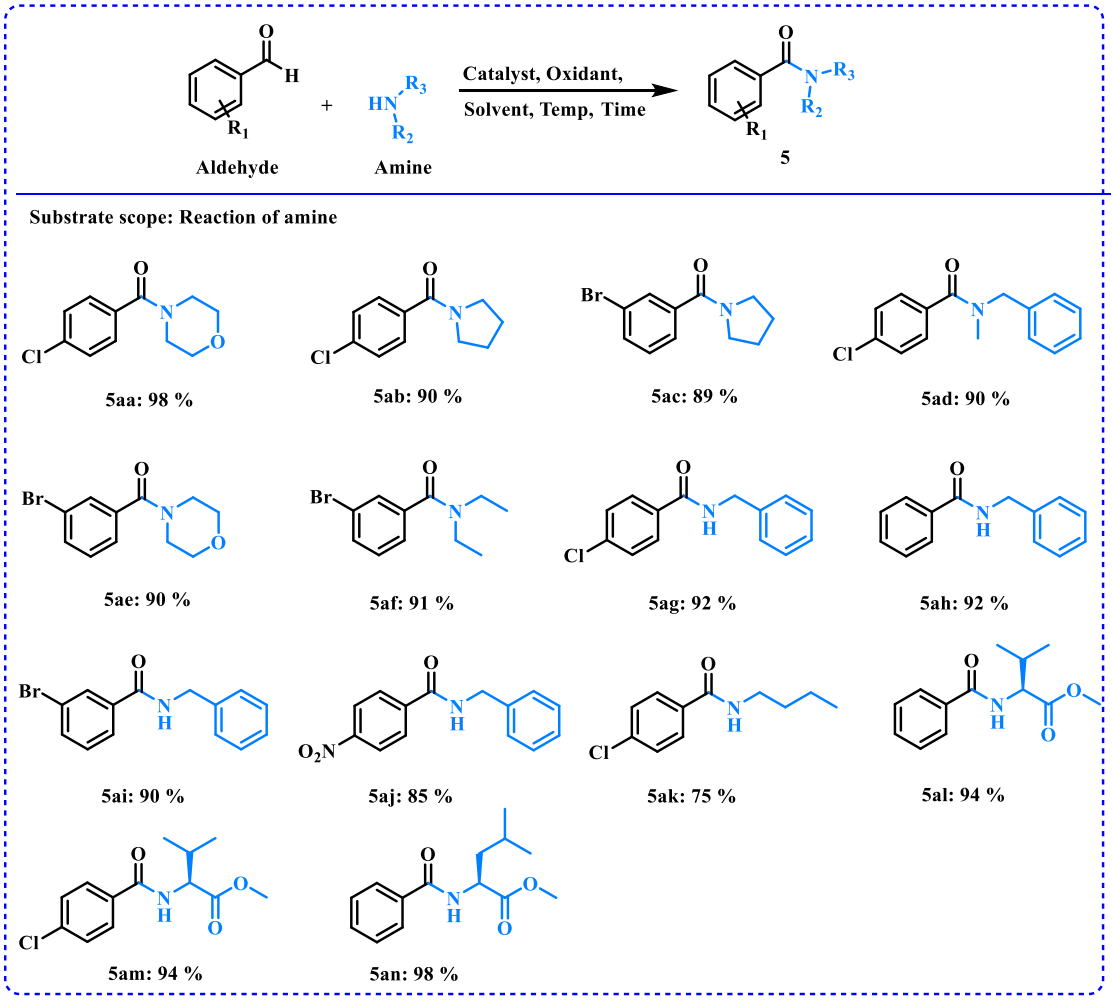

Scheme 5.3: Catalytic performance of NiO@Ni Mott-SChottky catalyst for amide bond formation. Reaction conditions: Aldehyde (1 mmol), amine (1 mmol), TBHP (4 mmol), NiO@Ni (5 mg), 1,4-dioxane (1 mL). Temperature: 60 °C, time: 8 h.

substitution of benzaldehyde partner (**Scheme 5.2, 5ad-5af, Table 5.2**). Interestingly, benzylamine produced amides in better yield than aliphatic primary amines (**Scheme 5.2, 5ag-5ak**).

The application of the amide bond formation was further extended to synthesize the peptides of amino acids. Methyl esters of valine and leucine produced corresponding amides with benzaldehyde and substituted benzaldehydes in an excellent yield, >94% (**Scheme 5.2, 5al-5an, Table 5.2**). This established the use of NiO@Ni as an efficient catalyst for peptide synthesis. Overall one equivalent of substituted benzaldehydes can be efficiently amidated with secondary amines, primary aliphatic, benzylic, and amino acid methyl esters in the presence of NiO@Ni.

5.9. Reaction mechanism and recyclability

It should be mentioned here that the catalyst NiO@Ni is magnetic and can be separated from the reaction mixture by using a magnet. Hence, we recovered the catalyst NiO@Ni and carried out the recycling experiments for the reaction of benzaldehyde with piperidine. A negligible decrease (8%) in yield was observed even after recycling the catalyst for five times (**Figure 5.3b**).

A tentative mechanism was proposed for the NiO@Ni catalyzed oxidative amidation of benzaldehydes. The reaction proceeds through a radical mechanism, as discussed earlier.[52] First, NiO@Ni catalyzed the homolytic cleavage of TBHP to form ^{t}BuO* and OH* radicals. Adsorption of substrates (amine and benzaldehyde) on catalyst surface facilitates the formation of corresponding radicals by reacting with ^{t}BuO* and/or OH* radicals. At last, the radical-radical coupling of acyl and amine radical takes place, resulting in the amide bond formation (**Figure 5.3a**).

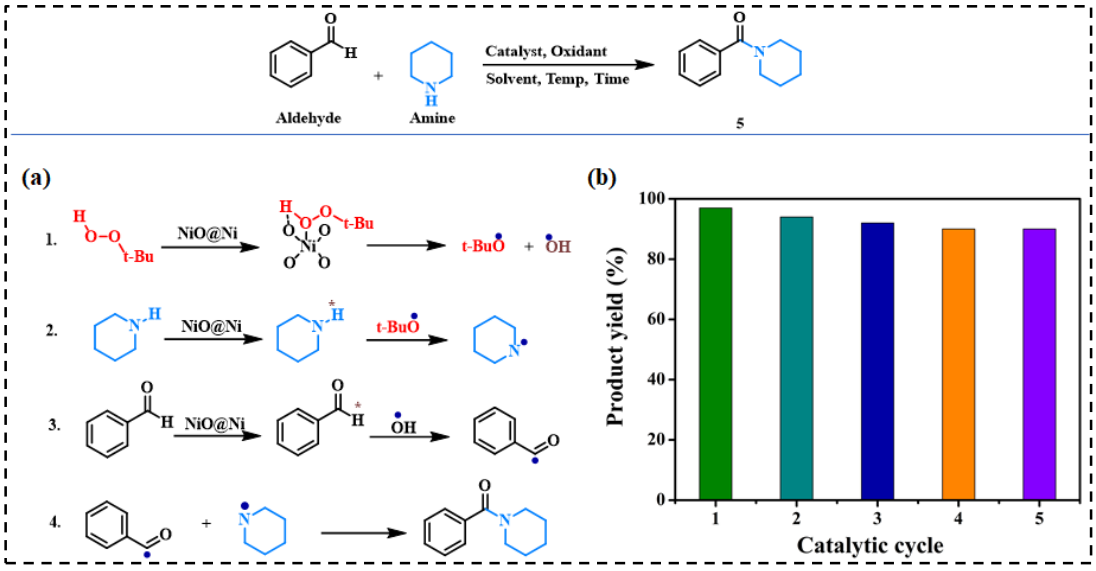

Figure 5.3. (a) Reaction mechanism for the amide bond formation reactions with the NiO@Ni catalyst and (b) recyclability graph of the NiO@Ni catalyst for the amidation reaction.

5.10. Conclusion

We have presented a facile approach for the synthesis of NiO@Ni Mott-Schottky catalyst through the calcination of Ni−Ni CP. The MOF-derived NiO@Ni Mott-Schottky catalyst exhibited significantly higher efficiency in catalyzing amide bond formation reactions compared to NiO@Ni nanoparticles obtained from nickel salt and commercially available NiO. The NiO@Ni catalyst proved to be robust in facilitating the formation of amides through reactions involving various benzaldehydes with diverse electron-donating and electron-withdrawing functional groups in *ortho*-, *meta*-, and *para*-positions, as well as a wide range of primary and secondary amines.

Table 5.2: ^{1}H NMR, ^{13}C NMR and spectra of the products[53],[54],[34],[55],[56]

Structure	Spectral Data
5a: phenyl(piperidin-1-yl) methanone 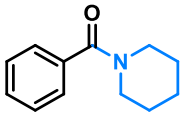	**^{1}H NMR** ($CDCl_3$, 500 MHz): δ 7.385 (s, 5H, Ar-H), 3.71 (bs, 2H), 3.336 (bs, 2H), 1.44-1.73 (m, 6H); **^{13}C NMR** ($CDCl_3$, 125 MHz): δ 170.34, 136.65, 129.34, 128.40, 126.8, 48.8, 43.15, 26.56, 25.65, 24.62;
5b: (4-methoxyphenyl) (piperidin-1-yl)methanone 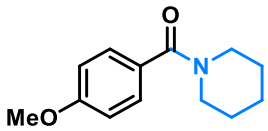	**^{1}H NMR** ($CDCl_3$, 500 MHz): δ 7.36-7.37 (m, 2H, Ar-H), 6.89-6.91 (m, 2H, Ar-H), 3.82 (s, 3H), 3.47-3.68 (m, 4H), 1.58-1.68 (m, 6H); **^{13}C NMR** ($CDCl_3$, 125 MHz): δ 170.31, 160.52, 128.86, 128.66, 113.63, 55.33, 24.67;
5c: (3-bromophenyl) (piperidin-1-yl) methanone 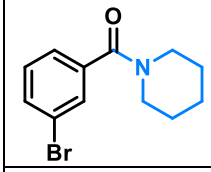	**^{1}H NMR** ($CDCl_3$, 500 MHz): δ 7.27-7.33 (m, 2H, Ar-H), 7.53-7.54 (m, 2H, Ar-H), 3.70 (br s, 2H), 3.33 (br s, 2H), 1.53-1.71 (m, 6H); **^{13}C NMR** ($CDCl_3$, 125 MHz): δ 168.54, 138.49, 132.42, 130.05, 129.88, 125.33, 122.57, 48.74, 43.20, 26.53, 25.56, 24.51;
5d: (4-chlorophenyl) (piperidin-1-yl) methanone 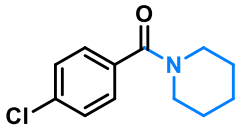	**^{1}H NMR** ($CDCl_3$, 500 MHz): δ 7.34-7.40 (m, 4H, Ar-H), 3.71 (br s, 2H), 3.34 (br s, 2H), 1.53-1.70 (m, 6H). **^{13}C NMR** ($CDCl_3$, 125 MHz): δ 169.24, 135.41, 134.86, 128.69, 128.38, 48.77, 43.24, 26.55, 25.58, 24.54.
5e: (2-hydroxyphenyl) (piperidin-1-yl) methanone 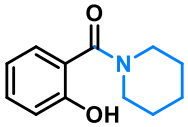	**^{1}H NMR** ($CDCl_3$, 500 MHz): δ 9.70 (br s, 1H), 7.29-7.32 (t, 1H, Ar-H), 7.22-7.24 (d, 1H, Ar-H), 6.98-7.00 (d, 1H, Ar-H), 6.819-6.851 (t, 1H, Ar-H), 3.64-3.66 (t, 4H), 1.63-1.71(m, 6H). **^{13}C NMR** ($CDCl_3$, 125 MHz): δ 170.88, 159.19, 132.52, 128.34, 118.55, 118.12, 117.50, 47.04, 26.25, 24.66.
5f:(2-nitrophenyl) (piperidin-1-yl) methanone 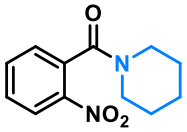	**^{1}H NMR** ($CDCl_3$, 500 MHz): δ 8.18-8.20 (m, 1H, Ar-H), 7.69-7.72 (m, 1H, Ar-H), 7.54-7.58 (m, 1H, Ar-H), 7.38-7.40 (m, 1H, Ar-H), 3.77 (d, 2H), 3.16-3.18 (t, 2H), 1.47-1.78 (m, 6H); **^{13}C NMR** ($CDCl_3$, 125 MHz): δ 166.25, 145.23, 134.42, 133.45, 129.57, 128.00, 124.74, 47.95, 42.74, 25.81, 25.13, 24.96.
5g: (4-nitrophenyl) (piperidin-1-yl) methanone 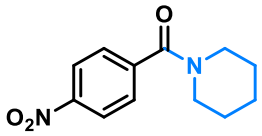	**^{1}H NMR** ($CDCl_3$, 500 MHz): δ 8.28-8.30 (d, 2H, Ar-H), 7.56-7.58 (m, 2H, Ar-H), 3.74 (br s, 2H), 3.30 (br s, 2H), 1.54-1.72 (m, 6H); **^{13}C NMR** ($CDCl_3$, 125 MHz): δ 167.90, 148.21, 142.72, 127.80, 123.86, 48.66, 43.21, 26.53, 25.51, 24.41.
5aa:(4-chlorophenyl) (morpholine) methanone	**^{1}H NMR** ($CDCl_3$, 500 MHz): δ 7.34-7.42 (m, 4H, Ar-H), 3.44-3.75 (m, 8H);

Structure	Spectral Data
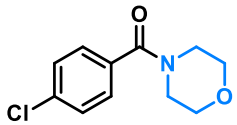	**^{13}C NMR** ($CDCl_3$, 125 MHz): δ 169.34, 135.99, 133.62, 128.86, 128.67, 66.81, 48.27, 42.75.
5ab: (4-chlorophenyl) (pyrrolidin-1-yl) methanone 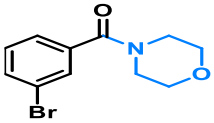	**^{1}H NMR** ($CDCl_3$, 500 MHz): δ 7.40-7.43 (m, 2H, Ar-H), 7.28-7.33 (m, 2H, Ar-H), 3.54-3.59 (m, 2H), 3.33-3.37 (m, 2H), 1.80-1.90 (m, 4H); **^{13}C NMR** ($CDCl_3$, 125 MHz): δ 168.47, 135.73, 135.53, 128.64, 128.44, 49.55, 46.25, 26.37, 24.36.
5ac: (3-bromophenyl) (pyrrolidin-1-yl) methanone 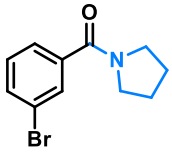	**^{1}H NMR** ($CDCl_3$, 500 MHz): δ 7.28-7.67 (m, 4H, Ar-H), 3.63-3.66 (t, 2H), 3.41-3.44 (t, 2H), 1.88-2.01 (m, 4H); **^{13}C NMR** ($CDCl_3$, 125 MHz): δ 167.99, 139.15, 132.81, 130.19, 129.93, 125.65, 122.38, 49.57, 46.27, 26.38, 24.43.
5ad: N-benzyl-4-chloro-N-methylbenzamide 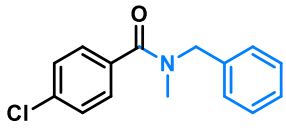	^{1}H NMR ($CDCl_3$, 500 MHz): δ 7.28-7.43 (m, 8H, Ar-H), 7.18 (s, 1H, Ar-H), 4.52-4.76 (d, 2H), 2.88-3.05 (d, 3H); ^{13}C NMR ($CDCl_3$, 125 MHz): δ 170.51, 135.74, 134.54, 128.74, 128.59, 128.37, 128.25, 127.69, 126.61, 55.16, 50.94, 37.00, 33.41.
5ae: (3-bromophenyl) (morpholine) methanone 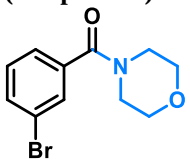	^{1}H NMR ($CDCl_3$, 500 MHz): δ 7.56-7.58 (m, 2H, Ar-H), 7.28-7.35 (m, 2H, Ar-H), 3.44-3.78 (m, 8H); ^{13}C NMR ($CDCl_3$, 125 MHz): δ 168.67, 137.27, 132.96, 130.20, 130.16, 125.61, 122.74, 66.82, 48.20, 42.66.
5af: N,N-diethylbenzamide 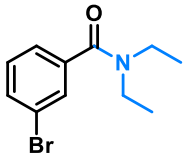	**^{1}H NMR** ($CDCl_3$, 500 MHz): δ 7.53-7.55 (m, 2H, Ar-H), 7.26-7.32 (m, 2H, Ar-H), 3.54 (br s, 2H), 3.26 (br s, 2H), 1.13-1.27 (m, 6H); **^{13}C NMR** ($CDCl_3$, 125 MHz): δ 169.52, 139.17, 132.19, 130.07, 129.41, 124.82, 122.54, 43.33, 39.38, 14.19, 12.86.
5ag: N-benzyl-4-chlorobenzamide 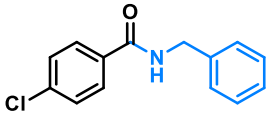	**^{1}H NMR** ($CDCl_3$, 500 MHz): δ 7.33-7.76 (m, 9H, Ar-H), 6.38 (s, 1H, N-H), 4.66-4.67 (d, 2H); **^{13}C NMR** ($CDCl_3$, 125 MHz): δ 166.26, 137.92, 137.84, 132.74, 128.88, 128.40, 127.99, 127.79, 44.28.
5ah: N-benzylbenzamide 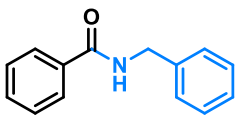	**^{1}H NMR** ($CDCl_3$, 500 MHz): δ 7.81-7.82 (m, 2H, Ar-H), 7.32-7.52 (m, 8H, Ar-H), 6.57 (br s, 1H, N-H), 4.65-4.66 (d, 2H); **^{13}C NMR** ($CDCl_3$, 125 MHz): δ 167.39, 138.23, 134.42, 131.55, 128.79, 128.60, 127.92, 127.62, 126.99, 44.14.

Structure	Spectral Data
5ai: N-benzyl-4-bromobenzamide 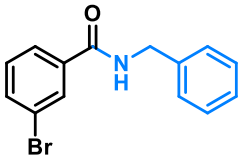	**^{1}H NMR** ($CDCl_3$, 500 MHz): δ 7.95 (t, 1H, Ar-H), 7.71-7.73 (m, 1H, Ar-H), 7.63-7.65 (m, 1H, Ar-H), 7.30-7.40 (m, 6H, Ar-H), 6.46 (br s, 1H, N-H), 4.64-4.65 (d, 2H); **^{13}C NMR** ($CDCl_3$, 125 MHz): δ 165.90, 137.84, 136.40, 134.53, 130.22, 130.18, 128.87, 127.98, 127.79, 125.56, 122.81, 44.30.
5aj: N-benzyl-4-nitrobenzamide 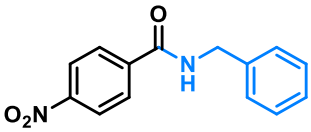	**^{1}H NMR** ($CDCl_3$, 500 MHz): δ 8.32-8.34 (d, 2H, Ar-H), 8.12-8.13 (d, 2H, Ar-H), 7.24-7.38 (m, 5H, Ar-H), 4.51-4.52 (d, 2H); **^{13}C NMR** ($CDCl_3$, 125 MHz): δ 165.08, 149.52, 140.43, 139.61, 129.25, 128.82, 127.78, 127.37, 124.05, 44.32.
5ak: N-benzyl-4-chlorobenzamide 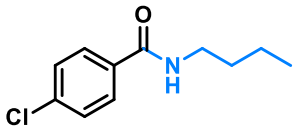	**^{1}H NMR** ($CDCl_3$, 500 MHz): δ 7.72-7.70 (d, 2H, Ar-H), 7.41-7.39 (d, 2H, Ar-H), 6.20 (NH), 3.47-3.30 (2H), 1.64-1.53 (2H), 1.46-1.34 (2H), 0.98-0.93 (3H); **^{13}C NMR** ($CDCl_3$, 125 MHz): δ 166.46, 137.51, 133.24, 128.76, 128.29, 39.39, 31.24, 19.97, 13.62.
5al: methyl benzoyl-L-valinate 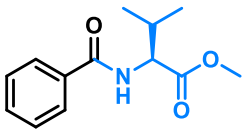	**^{1}H NMR** ($CDCl_3$, 500 MHz): δ 7.82-7.84 (d, 2H, Ar-H), 7.45-7.55 (m, 3H, Ar-H), 6.66-6.67 (d, 1H, NH), 4.80-4.82 (dd, 1H), 3.79 (s, 3H), 2.25-2.33 (m, 1H), 1.00-1.04 (m, 6H); **^{13}C NMR** ($CDCl_3$, 125 MHz): δ 172.69, 167.29, 134.18, 131.75, 128.64, 127.06, 57.41, 52.27, 31.66, 19.01, 17.97.
5am: methyl (4-chlorobenzoyl)-L-valinate 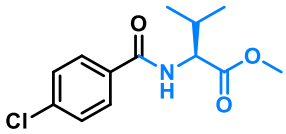	**^{1}H NMR** ($CDCl_3$, 500 MHz): δ 7.76-7.77 (m, 2H, Ar-H), 7.43-7.45 (m, 2H, Ar-H), 6.63-6.64 (d, 1H, NH), 4.77-4.79 (dd, 1H), 3.80 (s, 3H), 2.27-2.31 (m, 1H), 0.99-1.03 (m, 6H); **^{13}C NMR** ($CDCl_3$, 125 MHz): δ 172.62, 166.25, 138.02, 132.50, 128.89, 128.51, 57.50, 52.33, 31.63, 18.99, 17.98.
5an: methyl benzoyl-L-leucinate 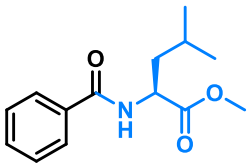	**^{1}H NMR** ($CDCl_3$, 500 MHz): δ 7.78-7.79 (m, 2H, Ar-H), 7.39-7.49 (m, 3H, Ar-H), 6.65 (s, 1H, NH), 4.84-4.88 (m, 1H), 3.75 (s, 3H), 1.66-1.76 (m, 3H), 0.95-0.98 (m, 6H); **^{13}C NMR** ($CDCl_3$, 125 MHz): δ 173.75, 167.13, 133.94, 131.72, 128.57, 127.08, 52.37, 51.14, 41.83, 25.00, 22.84, 22.05.

5.11. ^{1}H NMR and ^{13}C NMR spectra of the product

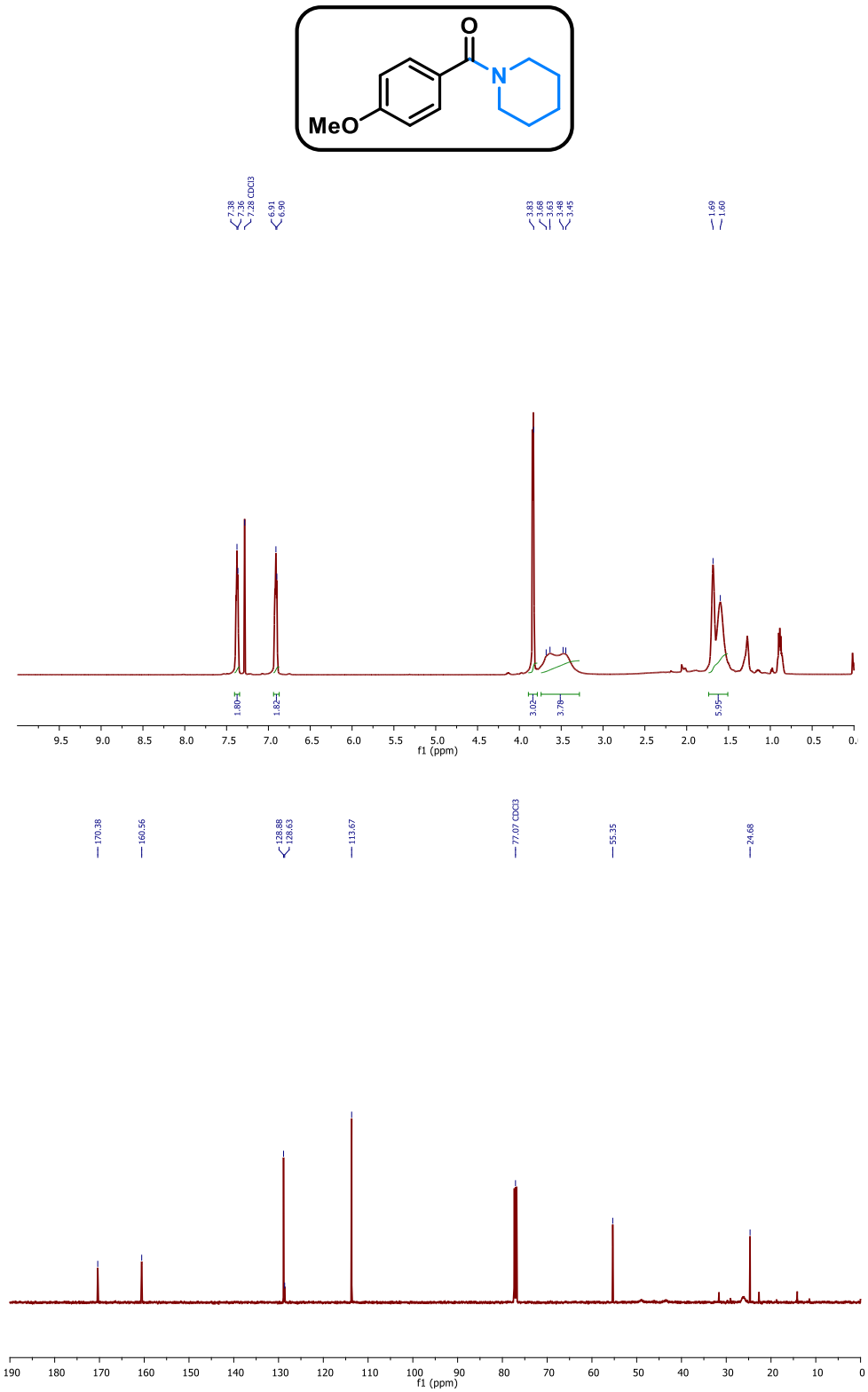

Figure 5.4: ^{1}H NMR and ^{13}C NMR spectra of the compound 5b.

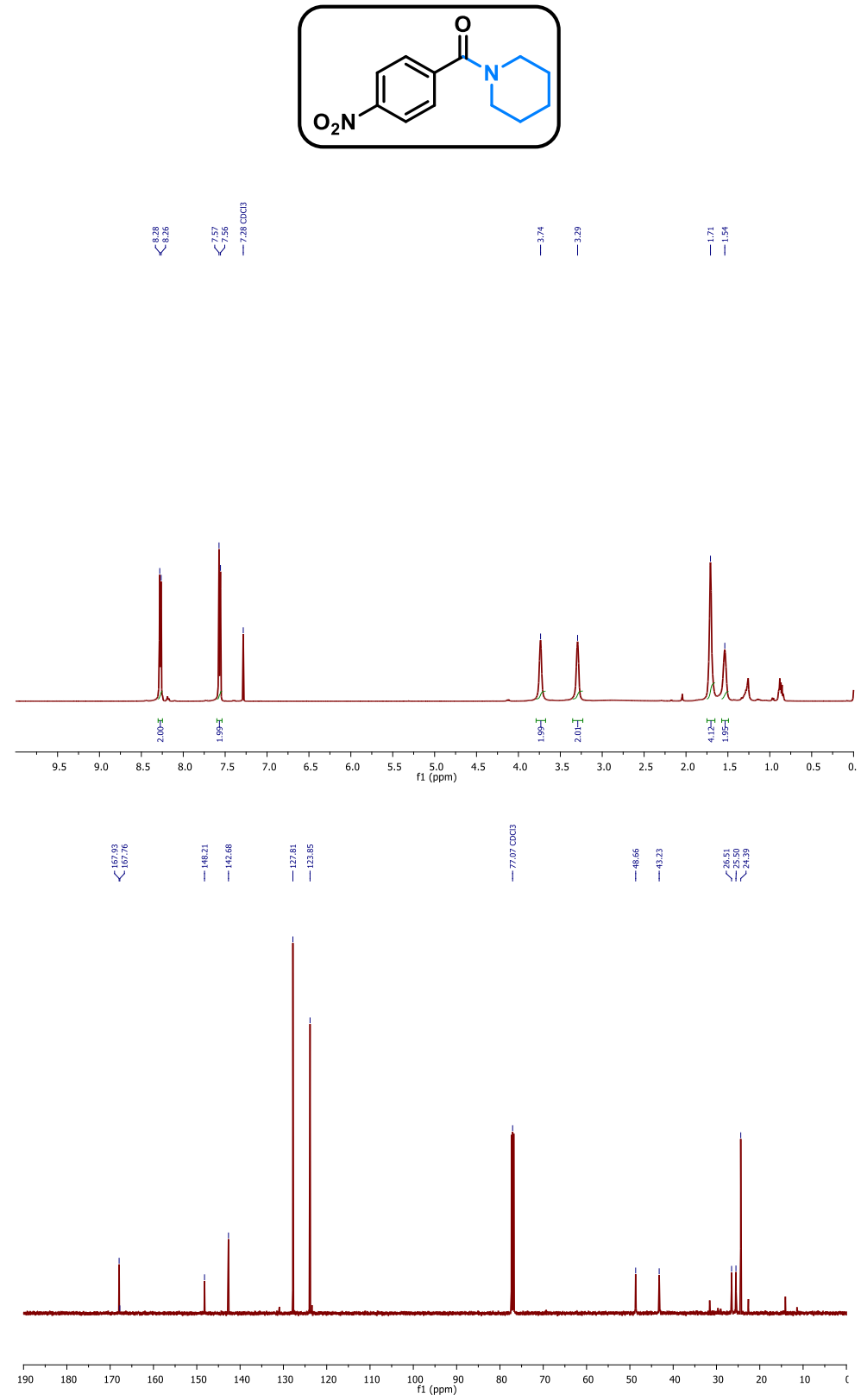

Figure 5.5: ^{1}H NMR and ^{13}C NMR spectra of the compound 5g.

5.12. References

[1] T. L. Luyen Doan, D. C. Nguyen, K. Kang, A. Ponnusamy, H. I. Eya, N. Y. Dzade, C. S. Kim, C. H. Park, *Appl. Catal. B Environ.* **2024**, *342*, 123295.

[2] H. Yang, B. Wang, S. Kou, G. Lu, Z. Liu, *Chem. Eng. J.* **2021**, *425*, 131589.

[3] H. Su, K. X. Zhang, B. Zhang, H. H. Wang, Q. Y. Yu, X. H. Li, M. Antonietti, J. S. Chen, *J. Am. Chem. Soc.* **2017**, *139*, 811–818.

[4] X. H. Li, M. Baar, S. Blechert, M. Antonietti, *Sci. Rep.* **2013**, *3*, 1743.

[5] D. G. Brown, J. Boström, *J. Med. Chem.* **2016**, *59*, 4443–4458.

[6] E. Valeur, M. Bradley, *Chem. Soc. Rev.* **2009**, *38*, 606–631.

[7] A. M. Whittaker, V. M. Dong, *Angew. Chem. Int. Ed.* **2015**, *54*, 1312–1315.

[8] T. Ben Halima, J. Masson-Makdissi, S. G. Newman, *Angew. Chem. Int. Ed.* **2018**, *130*, 13107–13111.

[9] S. Jamalifard, J. Mokhtari, Z. Mirjafary, *RSC Adv.* **2019**, *9*, 22749–22754.

[10] L. U. Nordstrøm, H. Vogt, R. Madsen, *Chemtracts* **2010**, *23*, 90–93.

[11] P. Yu, Y. Wang, Z. Zeng, Y. Chen, *J. Org. Chem.* **2019**, *84*, 14883–14891.

[12] L. Ren, X. Li, N. Jiao, *Org. Lett.* **2016**, *18*, 5852–5855.

[13] L. Liu, A. Corma, *Chem. Rev.* **2018**, *118*, 4981–5079.

[14] F. Li, Y. Qian, A. Stein, *Chem. Mater.* **2010**, *22*, 3226–3235.

[15] A. Indra, P. R. Rajamohanan, C. S. Gopinath, S. Bhaduri, G. K. Lahiri, *Appl. Catal. A Gen.* **2011**, *399*, 117–125.

[16] V. R. Pattabiraman, J. W. Bode, *Nature* **2011**, *480*, 471–479.

[17] D. Astruc, *Chem. Rev.* **2020**, *120*, 461–463.

[18] A. Indra, N. Maity, P. Maity, S. Bhaduri, G. K. Lahiri, *J. Catal.* **2011**, *284*, 176–183.

[19] A. Indra, C. S. Gopinath, S. Bhaduri, G. Kumar Lahiri, *Catal. Sci. Technol.* **2013**, *3*, 1625–1633.

[20] A. Indra, M. Doble, S. Bhaduri, G. K. Lahiri, *ACS Catal.* **2011**, *1*, 511–518.

[21] A. Indra, B. Singh, A. Yadav, *J. Mater. Chem. A* **2022**, *10*, 3843–3868.

[22] K. Patil, P. Babar, D. M. Lee, V. Karade, E. Jo, S. Korade, J. H. Kim, *Sustain. Energy Fuels* **2020**, *4*, 5254–5263.

[23] Y. Zeng, G. F. Chen, Z. Jiang, L. X. Ding, S. Wang, H. Wang, *J. Mater. Chem. A* **2018**, *6*, 15942–15946.

[24] R. V. Jagadeesh, K. Murugesan, A. S. Alshammari, H. Neumann, M. M. Pohl, J. Radnik, M. Beller, *Science.* **2017**, *358*, 326–332.

[25] A. Indra, T. Song, U. Paik, *Adv. Mater.* **2018**, *30*, 1–25.

[26] M. Jiang, Y. Li, Z. Lu, X. Sun, X. Duan, *Inorg. Chem. Front.* **2016**, *3*, 630–634.

[27] X. Han, L. Sun, F. Wang, D. Sun, *J. Mater. Chem. A* **2018**, *6*, 18891–18897.

[28] A. Indra, U. Paik, T. Song, *Angew. Chem. Int. Ed.* **2018**, *57*, 1241–1245.

[29] X. H. Li, M. Antonietti, *Chem. Soc. Rev.* **2013**, *42*, 6593–6604.

[30] R. Larouche-Gauthier, G. Bélanger, *Org. Lett.* **2008**, *10*, 4501–4504.

[31] M. B. Zakaria, M. Hu, R. R. Salunkhe, M. Pramanik, K. Takai, V. Malgras, S. Choi, S. X. Dou, J. H. Kim, M. Imura, S. Ishihara, Y. Yamauchi, *Chem. A Eur. J.* **2015**, *21*, 3605–3612.

[32] F. Zou, Y. M. Chen, K. Liu, Z. Yu, W. Liang, S. M. Bhaway, M. Gao, Y. Zhu, *ACS Nano* **2016**, *10*, 377–386.

[33] Y. Feng, X. Y. Yu, U. Paik, *Sci. Rep.* **2016**, *6*, 1–8.

[34] F. Messa, S. Perrone, M. Capua, F. Tolomeo, L. Troisi, V. Capriati, A. Salomone, *Chem. Commun.* **2018**, *54*, 8100–8103.

[35] H. Inagawa, S. Uchida, E. Yamaguchi, A. Itoh, *Asian J. Org. Chem.* **2019**, *8*, 1411–1414.

[36] M. Hu, S. Ishihara, Y. Yamauchi, *Angew. Chemie - Int. Ed.* **2013**, *52*, 1235–1239.

[37] X. Y. Yu, Y. Feng, B. Guan, X. W. D. Lou, U. Paik, *Energy Environ. Sci.* **2016**, *9*, 1246–1250.

[38] V. Biju, M. Abdul Khadar, *Spectrochim. Acta - Part A Mol. Biomol. Spectrosc.* **2003**, *59*, 121–134.

[39] M. B. Zakaria, C. Li, Q. Ji, B. Jiang, S. Tominaka, Y. Ide, J. P. Hill, K. Ariga, Y. Yamauchi, *Angew. Chem. Int. Ed.* **2016**, *55*, 8426–8430.

[40] M. Sookhakian, W. J. Basirun, M. A. M. Teridi, M. R. Mahmoudian, M. Azarang, E. Zalnezhad, G. H. Yoon, Y. Alias, *Electrochim. Acta* **2017**, *230*, 316–323.

[41] K. Wang, L. Li, H. Zhang, *Int. J. Electrochem. Sci.* **2013**, *8*, 5036–5041.

[42] J. Wang, S. Mao, Z. Liu, Z. Wei, H. Wang, Y. Chen, Y. Wang, *ACS Appl. Mater. Interfaces* **2017**, *9*, 7139–7147.

[43] G. Zhou, D. W. Wang, L. C. Yin, N. Li, F. Li, H. M. Cheng, *ACS Nano* **2012**, *6*, 3214–3223.

[44] X. Cao, Y. Shi, W. Shi, G. Lu, X. Huang, Q. Yan, Q. Zhang, H. Zhang, *Small* **2011**, *7*, 3163–3168.

[45] M. Zhou, H. Chai, D. Jia, W. Zhou, *New J. Chem.* **2014**, *38*, 2320–2326.

[46] H. Wang, H. Yi, X. Chen, X. Wang, *J. Mater. Chem. A* **2014**, *2*, 3223–3230.

[47] P. W. Menezes, A. Indra, O. Levy, K. Kailasam, V. Gutkin, J. Pfrommer, M. Driess, *Chem. Commun.* **2015**, *51*, 5005–5008.

[48] A. Indra, P. W. Menezes, K. Kailasam, D. Hollmann, M. Schröder, A. Thomas, A. Brückner, M. Driess, *Chem. Commun.* **2016**, *52*, 104–107.

[49] D. Bhattacharjya, H. Y. Park, M. S. Kim, H. S. Choi, S. N. Inamdar, J. S. Yu, *Langmuir* **2014**, *30*, 318–324.

[50] B. Singh, A. Indra, *Inorganica Chim. Acta* **2020**, *506*, 119440.

[51] R. Bernini, A. Coratti, G. Provenzano, G. Fabrizi, D. Tofani, *Tetrahedron* **2005**, *61*, 1821–1825.

[52] D. D. Subhedar, S. S. R. Gupta, B. M. Bhanage, *Catal. Letters* **2018**, *148*, 3102–3111.

[53] G. OMahony, A. K. Pitts, *Org. Lett.* **2010**, *12*, 2024–2027.

[54] S. Y. Lu, S. S. Badsara, Y. C. Wu, D. M. Reddy, C. F. Lee, *Tetrahedron Lett.* **2016**, *57*, 633–636.

[55] R. Balaboina, N. S. Thirukovela, R. Vadde, C. S. Vasam, *Tetrahedron Lett.* **2019**, *60*, 847–851.

[56] H. S. Casalongue, S. Kaya, V. Viswanathan, D. J. Miller, D. Friebel, H. A. Hansen, J. K. Nørskov, A. Nilsson, H. Ogasawara, *Nat. Commun.* **2013**, *4*, 3817.